Continuous Extraction Rate Measurements During Supercritical CO_2 Drying of Silica Alcogels

Submitted by
Justin S. Griffin

IN PARTIAL FULFILLMENT OF THE REQUIREMENTS FOR THE DEGREE OF

MASTER OF SCIENCE IN MECHANICAL ENGINEERING

School of Engineering
Tufts University
Medford, Massachusetts

February 2013

Certified by: Associate Professor Marc Hodes

Committee: Professor Chris Rogers
Professor Vincent Manno
Dr. George Gould

ABSTRACT

Modeling of Ethanol-Silica Alcogel Drying Using Supercritical Carbon Dioxide

by

Justin S. Griffin

Chair: Marc Hodes

Drying, specifically supercritical CO_2 ($SCCO_2$) -based drying, is a crucial step in the manufacture of silica aerogels and is also one of the most time and energy intensive. The aim of the present work is to elucidate the kinetics of this process in order to facilitate its acceleration. An apparatus was developed which is capable of continuously measuring ethanol extraction rates as a function of various process variables by three separate and redundant techniques. Results from experimental drying of 220 mm alcogel annuli (46 mm ID, 56 mm OD) are presented over a range of CO_2 flow rates from 1 kg/hr to 5 kg/hr. A concentric annular model was developed which considers the conjugate mass transfer problem of diffusion within the alcogel, with composition-dependent diffusivity, and convective flow over it. The model is shown to agree relatively well with experimental data.

Acknowledgments

First and foremost I would like to thank my advisor, Dr. Marc Hodes. Working with Dr. Hodes for the entirety my undergraduate and graduate research has been an entirely positive and formative experience, and his influence as an advisor and mentor cannot be understated. From intercontinental conference calls to research meetings derailed by culinary discussions, his knowledge and guidance is appreciated immensely.

I would also like to acknowledge my thesis committee members: Dr. Vincent Manno, Dr. Chris Rogers, and Dr. George Gould. They provided unique insights, and their advice helped strengthen my work and this thesis.

A number of my fellow graduate students are also deserving of thanks. Drew Mills and Martin Cleary designed and constructed the basis of my experimental apparatus with a great deal of skill and foresight, and Drew continually answered questions for me throughout the course of my research. Rui Zhang and Dave Brooks kept me company during long days in the lab, and helped me work through numerous experimental roadblocks. Ryan Nelson deserves more credit than I can express here for saving my thesis and, indeed, the entire aerogel research program. He came to the lab at all hours to ensure experiments could proceed on schedule, repeated an entire suite of my experiments on account of a faulty instrument, and ultimately the success of this project is a direct result of his insight and ingenuity.

I would like to thank the DOE (contract number DE-EE0000266) and our industrial partner Aspen Aerogels, specifically George Gould, Mez Polad, Shannon White, Sara Jarowowicz, and Redouane Begag for their support in establishing an aerogel research facility at Tufts University. My gratitude is also extended to Ann Anderson at Union College for use of her aerogel characterization facilities, and Stephen Steiner for sharing his valuable insight and experience.

Finally, I would like to thank my family and my fiancee for their constant support and reassurance, and for inspiring me to excel in everything I do.

TABLE OF CONTENTS

LIST OF FIGURES

Figure

LIST OF TABLES

Table

Nomenclature

d	characteristic length [m]
D	diffusivity $[\frac{m^2}{s}]$
k	thermal conductivity $[\frac{W}{mK}]$
Kn	Knudsen number
L	length of annular alcogel
M	mass [kg]
$\dot{m}$	mass flow rate $[frackghr]$
MW	molar mass $[fracgmole]$
p	pressure [MPa]
p_c	critical pressure [MPa]
p_r	reduced pressure [MPa]
P	parachor $[\frac{cm^3 g^{\frac{1}{4}}}{s^{\frac{1}{2}} mol}]$
P_{e_m}	Peclet number
R	universal gas constant $[\frac{j}{kmolK}]$
Re	Reynolds number
r_p	pore radius [nm]
S_s	specific surface area [m^2/g]
t	time [s]
T	temperature [K]
T_c	critical temperature
T_r	reduced temperature

u	velocity $[\frac{m}{s}]$
V	molar volume $[cm^3/mol]$
w	mass fraction
x	mole fraction

Greek Symbols

μ	viscosity [cP]
ϕ	Porosity [%]
ρ	density $[\frac{kg}{m^3}]$
σ	surface tension $[\frac{mN}{m^2}]$
Σ_v	sum of diffusion volumes

Subscripts

c	critical value
C	carbon dioxide
E	ethanol
eff	effluent
F	overall fluid property
IR	measured by IR sensor
l	liquid phase
r	reduced value
v	vapor phase

Superscripts

6$\circ$	infinite dilution value

Acronyms

$SCCO_2$	supercritical carbon dioxide
SCD	supercritical drying

CHAPTER I

Introduction

Aerogels, sometimes referred to as "frozen smoke" and best known for their usage as (thermal) "superinsulators," are dry, porous, and amorphous nanostructured materials with unique thermophysical properties. Silica (SiO_2)-based aerogels, subsequently referred to as aerogels, are most common, and considered here. Background material on their manufacture, properties, and applications is followed by discussion on supercritical carbon dioxide ($SCCO_2$) drying of alcogels, a common step in aerogel manufacture. Then, an apparatus and procedure to continuously measure alcohol extraction rates during $SCCO_2$ drying of alcogels are described. Next, measured extraction rates as a function of mass flow rate of CO_2 are presented and the measured material properties of a representative aerogel provided. Finally, the data are compared to the predictions of a numerical model which considers the conjugate mass transfer problem of diffusion of alcohol through the alcogel and advective mass transfer into an adjacent CO_2 stream.

1.1 Silica Aerogel

1.1.1 Manufacture

The primary steps in aerogel manufacture are gelation, ageing and drying. In the usual gelation step, catalyst and a water – silicon alkoxide solution in an alcohol solvent causes

formation of a nanostructured silica skeleton by hydrolysis, (water and alcohol) polycondensation, and crosslinking [**?**]. The pores of the resulting alcogel (or more generally wet gel) are (predominantly) filled with alcohol and both phases are continuous. Next, ageing of the alcogel increases the mechanical strength of its skeleton. During ageing hydrolysis and condensation reactions continue at a modest rate, particle clusters collide on account of Brownian motion and combine [**?**], and silica is transported to the neck regions within the skeleton on account of the dependence of its solubility in the pore liquid on the radius of curvature of solid-liquid interfaces [**?**]. Syneresis, i.e., shrinking of the alcogel and expulsion of the pore fluid, may also occur [**?**]. Alcogel immersion in alcohol during ageing purifies the pore fluid. Ageing may be accelerated by elevated temperature, pH adjustment and/or water addition.

Drying the wet gel, i.e., replacing the pore fluid by air, is the last manufacturing step and has been reviewed by Bisson [**?**] *et al.* Evaporation of the pore fluid at ambient conditions results in severe shrinkage and cracking of the (relatively weak) skeleton and the formation of xerogel due to large capillary forces caused by nearly perfect wetting of silica by alcohol due to the presence of an adsorbed liquid layer on it [**?**] and nm-scale pore radii. However, other drying methods preserve the delicate skeletal structure in a wet gel to produce an aerogel.

Hydrogels (i.e., those where the pore fluid is water) prepared from low-cost sodium silicate precursors may be dried by ambient pressure drying (APD), albeit at elevated temperature [**?** **?**]. However, intermediate steps, i.e., salt removal by washing, hydrogel to alcogel conversion by solvent exchange and surface modification to reduce capillary stresses during evaporation, are standard practice and a low degree of monolithicity is achieved. Freeze drying has also been considered and, recently, Pons *et al.* [**?**] published a study on the first (rather brittle) monoliths (up to 950 mm^3 in volume) produced by it.

Larger monoliths may be obtained by supercritical drying, the technique used by Kistler [**?**] to produce the first aerogel. In direct supercritical drying, a phase boundary within the

wet gel and thus capillary stress are avoided by slowly heating it above its critical temperature (241°C in the case of ethanol (EtOH)) in an autoclave before slow depressurization. Modern variants of this process exist [**?** **?**], but flammability remains a concern in the case of alcogels. Supercritical-CO_2 ($SCCO_2$) drying, the subject of this paper and perhaps the most common method, is discussed in Section 1.2.

1.1.2 Properties

The skeletal material of aerogel is composed of interconnected nm-scale silica particles with a density slightly below that of amorphous silica (2200 kg/m^3) [**?**]. Typically, porosity (ϕ) is above 90%, pore sizes range from 5 nm to 100 nm and mean pore size between 20 nm to 40 nm [**?** **?**]. Typical bulk densities ranges for "low-, medium- and high-density" aerogels are 3 kg/m^3 to 10 kg/m^3 (below any other solid), 10 kg/m^3 to 100 kg/m^3, and 100 kg/m^3 to 500 kg/m^3, respectively [**?** **?**]. Typical specific surface area (S_s) is rather high, ranging from 250 m^2/g to 800 m^2/g. Aerogel can be made transparent [**?**] and hydrophobic to prevent deterioration when exposed to humid air [**?**].

Heat transfer through silica aerogel occurs by conduction through the silica skeleton and the air contained in its pores as well as radiation and its effective thermal conductivity accounts for all three mechanisms. (Natural convection is irrelevant due to the length scale of the pores.) Conduction through the silica skeleton is limited by a tortuous path through a high porosity medium with many "dead-ends" and that through the air is degraded because it does not behave as a continuum. The mean-free path of air at atmospheric conditions, say, 20°C, 1.01325 x 10^5 Pa and arbitrary relative humidity, is 65 nm [**?**]. Hence, the Knudsen number (Kn = mean free path/mean pore size) for typical silica aerogels ranges from about 1.5 to 3. The transitional flow regime (i.e., that between the continuum slip and free molecular flow regimes) exists when 0.1 <Kn <10 [**?**] and analysis of conduction and convective heat transfer in this regime necessitates the application of statistical methods to groups of molecules [**?**]. At atmospheric conditions the air in the vast majority of

the pores of a silica aerogel is in the transitional regime and the silica skeleton degrades conduction by obstructing the energy exchange between gas molecules. Measurements by Zheng *et al.* [**?**] showed that the thermal conductivity of the air in a representative silica aerogel (ϕ = 94 %, ρ = 110 kg/m^3 and S_s = 797 m^2/g) was 0.01 W/(m·K) at 1 bar and decreases to essentially zero under moderate vacuum (0.01 bar). (The thermal conductivity of air at atmospheric conditions is 0.024 W/(m·K)). Measurements by Duer and Svendsen [**?**] of the effective thermal conductivities (k_e) of four representative silica aerogels under evacuated conditions, where heat transfer is exclusively attributable to conduction through the skeleton and radiation, showed that it ranges from 0.090 W/(m·K) to 0.011 W/(m·K). It ranged from 0.015 W/(m·K) to 0.017 W/(m·K) under non-evacuated conditions, implying the thermal conductivity of the air was about 0.06 W/(m·K).

The effective thermal conductivity reported for commercially available silica aerogel insulation is in-line with the aforementioned laboratory results. For example, Spaceloft®, manufactured by Aspen Aerogels (Northborough, MA), is a flexible blanket infused with silica aerogel with an effective thermal conductivity of 0.015 W/(m·K). This is considerably below that of the highest performance (non-evacuated) commercially available insulation, i.e., polymer foams, $k_e \gtrsim$ 0.020 W/(m·K) [**?**]. Utilization of vacuum insulation panels (VIPs) and vacuum glazing (VG) results in effective thermal conductivities as low as 0.003 W/(m·K) and 0.00001 W/(m·K), respectively, [**?** **?**]. However, both are subject to degradation as air permeates the vacuum over time and, unlike aerogel, are load bearing strucures and lose their insulating quality if punctured.

1.1.3 Applications

As of 2009 silica aerogel was about 20 times as expensive as conventional insulation [**?**] per unit of thermal resistance; therefore, its use has been limited to niche applications. For example, thermally-insulating insoles are not viable using conventional insulation due its required thickness and weakness in compression [**?**]. However, due to an embedded

layer of Spaceloft®, Toasty Feet® insoles are sufficiently thin and strong in compression [**?**]. Moreover, aerogel is often used to insulate off-shore oil and gas pipelines to reduce their diameter. Then ships may carry longer lengths of pipeline thereby reducing transport and thus installation cost [**?**]. Going forward, the most promising application for aerogels is in the insulation of buildings. Indeed, in the United States cooling and heating of buildings accounts for 15 % of energy consumption [**?**] and, subject to them becoming economically feasible, aerogels (unlike renewable energy) may immediately and substantially reduce this consumption and the concomitant CO_2 emissions. Other applications of aerogels are summarized by Garca-Gonzlez *et al.* [**?**] and include, e.g., their use as oxygen sensors via doping them with oxygen-sensitive molecular probes and measuring fluorescence intensity [**?**] and aerosol collection in a transparent medium [**?**].

1.2 Supercritical CO_2 Drying

The first step in the usual $SCCO_2$ drying (batch) process is replacement of alcohol within an alcogel with liquid CO_2 by solvent exchange. Then, the wet gel is heated in a pressure vessel until the CO_2 becomes a supercritical fluid, i.e., its critical temperature (31.1 °C) and critical pressure (7.39 MPa) are exceeded. Next, the CO_2 is slowly depressurized (to avoid cracks in the silica skeleton) while maintaining the system above the critical temperature to avoid the formation of a phase boundary. Finally, the gel is exposed to the atmosphere and air replaces the gaseous CO_2 resulting in an aerogel. In some cases, including the present study, the solvent exchange step is skipped [**?**]. Unlike direct supercritical extraction $SCCO_2$ drying is a low temperature and nonflammable process.

Studies on $SCCO_2$ drying have been motivated by the required capital investment in pressure vessels (albeit less than for direct supercritical extraction), time (several hours is typical) and energy associated with pressurization, heating and CO_2 recovery. Bypassing the solvent exchange step, van Bommel and de Haan [**?**] dried 1.5 cm diameter x 18 cm long (ethanol filled) alcogel rods initially submerged in excess ethanol at temperatures ranging

from 35 °C to 70 °C. Supercritical CO_2 was pumped through the autoclave at a rate of 1.0 kg/hr to 1.3 kg/hr. Crack-free aerogels were observed only when pressure was maintained above the mixture critical pressure of the CO_2-ethanol binary system, 75 bar at 35°C and monotonically increasing to 135 bar at 70 °C. Required drying time was estimated by varying the duration of the drying phase while holding all other process conditions constant and inspecting the final aerogel for cracks. Increasing the operating temperature and pressure from 85 bar and 35 °C to 140 bar and 70 °C reduced the required drying time from 3 hours to 2 hours and 45 minutes, a modest amount. Therefore, it was concluded that low-temperature drying is most economical. Subsequently, in a 1995 study, van Bommel and de Haan [**?**] concluded that 1 cm-thick aerogel sheets could be dried for 1.2 US dollars per square meter footprint.

Masmoudi *et al.*[**?**] formed 5.5 cm x 5.5 cm x 1 cm isopropanol (IPA)-based alcogels in teflon molds, aged them for 11 days (while purifying the IPA) and dried them (two at a time) in an autoclave (with an internal volume of 1 liter, initially filled with IPA [**?**]) maintained at 37.5 °C and 80 bar. Supercritical CO_2 at (non-constant) mass flow rates between 3 kg/hr and 9 kg/hour was pumped through the autoclave and, periodically, fluid was sampled in the vicinity of the alcogel, vaporized and injected into a gas chromatograph to measure IPA concentration. The duration of the drying phase, defined as the time when the IPA concentration reached the detection limit of the chromatography system (i.e. 5.6×10^{-5} kg/m^3) was 9200 $\pm$ 350 s. The effective (mean) diffusion coefficient for the IPA-CO_2 system at 37.5 °C and 80 bar was estimated to be 5.75 x 10^{-9} m^2/s by fitting the solution of an analytical diffusion model to the experimental data.

Wawrzyniak *et al.* [**?**] dried 0.9 cm diameter x 6.3 cm long rods of (ethanol filled) alcogel in a rocking autoclave (of internal volume 15 times that of the alcogel, initially filled with methanol) maintained at a pressure of 90 bar. $SCCO_2$ mass flow rate was constant at 0.3 kg/hr. Ethanol concentration in the effluent was measured chromatographically every 3 minutes. A one-dimensional, transient and analytical diffusion model was applied to the

alcogel rod under the assumption of zero ethanol concentration along its outer diameter. (Subsequently, Wawrzyniak *et al.* [**?**] relaxed this assumption and showed it only modestly influenced their results.) The fluid surrounding the alcogel was assumed to be well mixed and the concentration of ethanol within it numerically computed as a function of time. Effective (mean) diffusion coefficients yielding the best match between data and model ranged from 3.05 x 10^{-9} m^2/s to 5.52 x 10^{-9} m^2/s as autoclave temperature was increased from 20 °C to 42 °C.

Garca-Gonzlez *et al.* [**?**] dried 1.2 cm diameter x 3 cm long, i.e., 3.39 ml, (ethanol filled) alcogel rods submerged in 14 ml of excess ethanol in a 1.43 cm diameter x 15.94 cm long (nominaly 25 ml) tubular autoclave at a temperature of 318 K and pressure "up to 11.0 MPa." The mass flow rate of CO_2 into the autoclave was 0.24 kg/hr. A flow restrictor separated the effluent into an ethanol-rich liquid stream collected in vials and a CO_2-rich gaseous stream. Ethanol densities up to 2.5 mg/l (about 0.001 ethanol mass fraction at ambient conditions) in the gas stream were measured using a Dräger Alcotest 6810 breathalyzer. Subsequent to removal of the excess ethanol it was asserted that "spillage," i.e., ethanol removal from the gel due to it swelling from dissolution of CO_2 as dicussed by Mukhopadhyay and Rao [**?**], rapidly caused 92 % to 95 % of the ethanol in the alcogel to be replaced by CO_2 and was followed by slow diffusion-limited extraction of the remainder. Credence to this assertion was provided by observation of considerably faster drying of an equivalent mass of 183.3 μm (mean) diameter alcogel microspheres, where the length scale for diffusion is about 30 times less than that for the rods. Effective mean diffusion coefficients computed by Garca-Gonzlez *et al.* [**?**] were about twice those in the foregoing studies and this was attributed to possible variations in skeletal structure, experimental setup, and measurement technique.

There are key differences between the foregoing experiments and those considered here. First, we consider (laminar) internal flow of a $SCCO_2$ stream through an annulus concentric with an annular alcogel. Secondly, the alcogel occupies nearly half of the free volume of the pressure vessel as opposed to a small fraction of it. Thirdly, the alcogels are not initially

submerged in excess ethanol. Lastly, the concentration of ethanol in the efflucent is measured continuously and by redundant techniques.

CHAPTER II

Experiments

2.1 Alcogel Preparation

2.1.1 Sol-Gel Chemistry

Alcogels are produced by a two step (acid-base) sol-gel process [**? ? ?**] to afford control over the gel time and, ultimately, structure, composition and properties of the aerogel. The alcogels are strong enough to retain their shape during ageing without being so dense that forces which arise during syneresis cause rupture.

The first step (A) in gelation is partial hydrolysis of tetraethoxysilane (TEOS), a liquid precursor of silica, in a sub-stoichiometric amount of deionized water in the presence of acid catalyst. A solution of TEOS : EtOH : H_2O : HCl in the molar ratio 1 : 1.57 : 1.40 : 0.0007 with target hydrolysis of 70 % was prepared in a beaker, covered to minimize evaporation and stirred at low speed for 20 – 24 hours at 20 °C to form a colloidal solution, or sol.

The second step is the combination of the step A sol with a basic catalyst to promote condensation and, subsequently, gelation. First, the step A sol is diluted in ethanol and combined with additional water, attaining a TEOS : EtOH : H_2O : HCl molar ratio of 1 : 5.44 : 7.59 : 0.0007 (step B). Simultaneously, a basic catalyst mixture (12 % 14.5 M NH_4OH and 88 % ethanol by volume) is prepared. Finally, the step B sol and basic catalyst are combined in a sol : catalyst ratio of 8 : 1 (by volume). The overall TEOS : EtOH : H_2O

: HCl : NH_4OH molar ratio is 1 : 6.70 : 7.84 : 0.0007 : 0.19. Gel time of the diluted sol-base catalyst solution is 3 minutes ± 15 seconds and, ultimately, it produces aerogels with a density of about 80 kg/m^3.

Sources of TEOS and EtOH were Silbond® EG of (mininum) 99.8 % purity and non-denatured ethanol of 99.5 % purity from Silbond Corporaton and Spectrum Chemical Corporation, respectively. 12.1 M hydrochloric acid and 14.5 M ammonium hydroxide were both purchased from Sigma-Aldrich.

2.1.2 Casting and Aging

Once the diluted sol-base catalyst solution is mixed, it is poured into an annular mold for casting. The mold consists of an aluminum rod with circular end caps surrounded by a plastic annulus lined with Saran® wrap that is removed after gelation. The annulus of alcogel is aged twice in 4 times its volume of pure ethanol at 65 °C for 8-12 hours and subsequently stored in ethanol for up to one week.

2.2 Apparatus and Test Section

A schematic showing the primary components in the apparatus to measure the rate of ethanol extraction from the alcogel during $SCCO_2$ drying is shown in Figure 2.1. Temperature, pressure, CO_2 mass flow rate, and dimensions of the alcogel annulus and concentric annulus for the flow of CO_2 are variable; however, only CO_2 mass flow rate and inner diameter of the alcogel annulus are varied in this study.

Liquid CO_2 is supplied to the system from a dip tube in a cylinder (1) of (bone dry, minimum purity 99.9 %) CO_2 at ambient temperature and saturation pressure (about 5.7 MPa). It is sub-cooled (2) to below 5 °C to ensure only liquid enters a Hydraulics International Inc. 3L-SS-25 piston pump (3) driven by regulated cylinders of N_2 gas which increases its pressure to a maximum of 17.2 MPa. Next, the CO_2 is heated (4) above the mixture critical temperature of the ethanol-CO_2 system and passes through a Tescom 44-1164-24-259

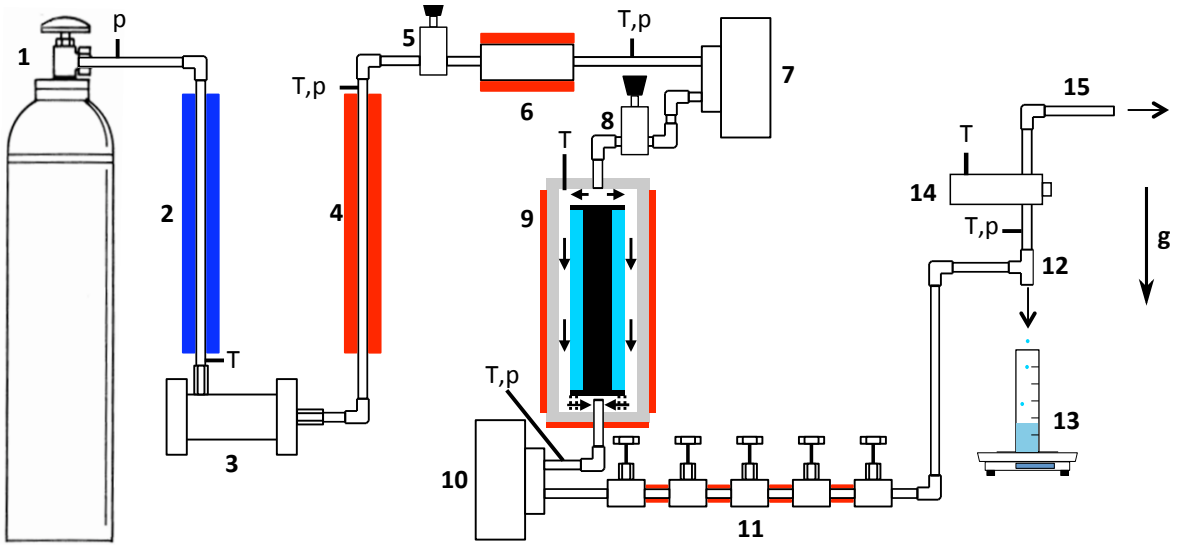

Figure 2.1: Schematic of apparatus. 1) CO_2 supply, 2) subcooler, 3) nitrogen-driven piston pump, 4) CO_2 heater, 5) primary pressure regulator, 6) heated accumulator, 7) CO_2 Coriolis flow meter, 8) secondary pressure regulator, 9) extraction vessel, 10) effluent Coriolis flow meter, 11) heated decompression valves, 12) effluent phase separator, 13) liquid ethanol collection on digital scale, 14) IR ethanol vapor sensor, 15) CO_2 - ethanol gaseous exhaust. Temperature and pressure measurement locations are indicated by "T" and "p," respectively.

forward-pressure regulator (5) and heated accumulator (6) which partially suppress pressure fluctuations from the cycle of the pump. Then, the CO_2 flows through a Siemens SITRANS F C MASS 2100 DI 1.5 Coriolis flow meter (7) connected to a Siemens SITRANS F C MASS 6000 for signal processing, where mass flow rate and density are measured to within $\pm$ 0.1 % of reading and $\pm$ 1 kg/m^3, respectively. CO_2 then flows through a second regulator (8) which sets the extraction pressure and further damps out pump pressure fluctuations before it enters the test section.

The CO_2 stream then enters a 7.62 cm inner diameter x 25.56 cm tall (1.165 liter) heated pressure vessel (9) custom manufactured from stainless steel (316 grade) by CF Technologies (Hyde Park, MA). 10 mm standoffs on the bottom endcap of the aluminum mandrel supporting the 4.62 cm inner diameter x 5.62 cm outer diameter x 22.0 cm tall annulus of alcogel position it in the center of the pressure vessel. The CO_2 impinges on the top endcap of the mandrel and then flows through the 1 cm annular gap surrounding the gel

as per Figure 2.1. A CO_2-ethanol mixture exits the pressure vessel through an exhuast tube (7 mm inner diameter) which protrudes through the base and into the vessel. The inlet of this tube is 20 mm above the bottom of the pressure vessel in order to prevent any excess liquid ethanol which may pool at the bottom of the vessel from leaving the vessel as a plug and overwhelming the effluent IR sensor. The mixture then flows through a second Coriolis flow meter (10). A series of five decompression valves (Swagelok SS-31-RS4) (11) reduce the pressure of the effluent to nearly atmospheric pressure. The valves are heated to prevent freezing due to Joule-Thomson cooling, which would damage their seals. It then flows into a tee-junction (12) with vertically oriented exits such that liquid drains from the junction and is collected in a covered beaker on a continuously-recording Ohaus Scout digital scale (13). The gaseous effluent stream flows through the other leg of the tee-junction into an infrared absorption-based hydrocarbon detector (SEC Millenium, model number 142-0280) (14) from Sensor Electronics Corporation (Edina, MN) which measures the ethanol content up to a maximum of 90 g/m^3 to within $\pm$ 4.5 g/m^3 (custom scale as per personal correspondence with SEC [**?**]). Finally, the gas/vapor exhaust is vented to a fume hood (15).

Temperature and pressure throughout the system are measured using T-type thermocouples (accurate to $\pm$ 1.0 °C), PX-309 pressure transducers (high pressure, $\pm$ 51.5 kPa), and PX-209 pressure transducers (low pressure, $\pm$ 0.52 kPa), all from Omega, at the points indicated in Figure 2.1. Further details on the system are provided by Mills [**?**].

2.3 Procedure

The first step in the experimental procedure is to preheat the pressure vessel to the extraction temperature and pre-pressurize the CO_2 supply line upstream of the extraction vessel pressure regulator in order to minimize the time the wet alcogel spends inside the vessel before reaching process temperature and pressure. Next, an alcogel sample is placed inside the the vessel, which is sealed rapidly using the Dur-O-Lok pressure vessel closure (which typically takes 30 seconds to close, as opposed to minutes required by traditional

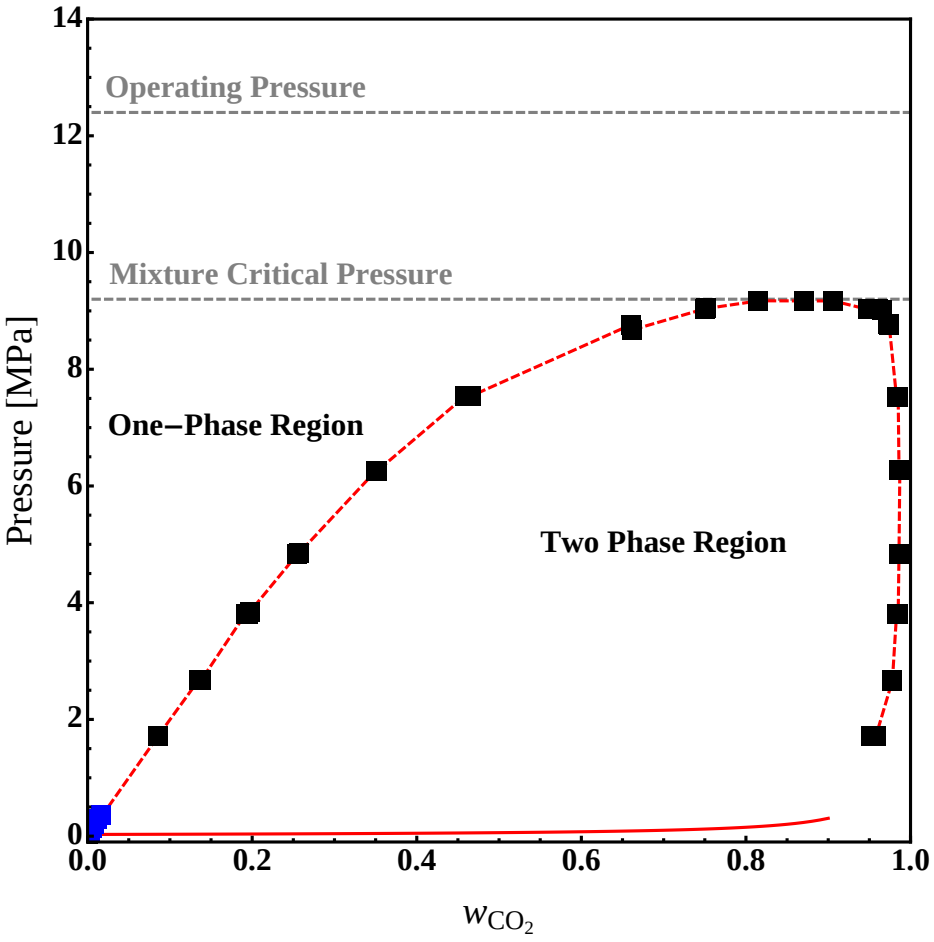

Figure 2.2: CO_2-ethanol system at 323 K [**?** **?**]. The system must remain in the one-phase region for the duration of the extraction process.

bolt closures). The extraction vessel is then pressurized by gradually opening the pressure regulators with the decompression valves closed. Because the wet gels are not submerged in excess ethanol, the pressurization time must be minimized . If substantial mass transfer is allowed to occur before mixture critical conditions are reached the fluid within the gel will enter the two-phase region shown in Figure 2.2, and stresses due to the resulting phase boundary will likely damage the gel [**?**]. However, pressurizing too rapidly could mechanically damage the gels. In the present case, where the primary concern is not maximizing optical transparency or overall monolithicity, a pressurization rate of 20 kPa/s to 40 kPa/s (i.e. 5 min to 10 min pressurization time) was found to be satisfactory.

Once the pressure within the extraction vessel is stabilized, the effluent decompression valves are opened and adjusted until the desired flow rate is reached. At this point, fine adjustments are made to the extraction pressure using the secondary pressure regulator, which is then left untouched for the duration of the experiment. CO_2 mass flow rate is corrected periodically by adjusting the decompression valves in the effluent line in order to maintain a relatively constant flow rate ($\pm$ 10% of set value). Flow rate adjustments are made as seldom as possible, as they result in spikes in the measured extraction rate.

The extraction phase ends when the mole fraction (x_e) measured by the IR sensor reads $x_E < 0.001$ for 20 minutes, at which point depressurization begins. Pressure is reduced by shutting off the pump and CO_2 supply while leaving the effluent valves open, thus purging the vessel through the effluent flow meter. During decompression the system is continuously heated so that conditions remain isothermal within the extraction vessel allowing the fluid within the gel to pass from a supercritical state to a gaseous state without the formation of a liquid-vapor phase boundary. As in the pressurization phase is also important that decompression not occur too rapidly, owing to the low permeability of the gels. If the gas within the pores expands more quickly than it can escape from the gel significant cracking can occur [**?**]. The depressurization rate is typically comparable to the pressurization rate.

2.4 Material Characterization

Aerogels prepared by the method described herein were analyzed at Union College (Schenectady, NY). Physiorption testing was performed on a Micromeritics ASAP 2010, which produced N_2 adsorption/desorption isotherms. These isotherms were analyzed using the BET (Brunauer-Emmett-Teller) method [**?**] and the surface area was calculated was 927 $m^2/g \pm 9$ m^2/g. The average pore diameter, determined using the BJH (Barrett-Joyner-Halenda) method [**?**], was 19.8 nm based on the adsorption isotherm and 15.3 nm based on the desorption isotherm. Thermal conductivity was measured using a Hot Disk Thermal Constants Analyzer. The samples had an average thermal conductivity of 0.043 w/mK.

2.5 Data Reduction

2.5.1 Instantaneous Extraction Rate

Ethanol extraction rate is measured continuously by two separate and redunant methods. The primary method is to use the combined data from the two effluent streams (gaseous and condensed). The total ethanol extraction rate is

$$\dot{m}_E = \dot{m}_{E,v} + \dot{m}_{E,l} \tag{2.1}$$

where $\dot{m}_{E,v}$ is the mass flow rate of ethanol measured in the vapor phase and $\dot{m}_{E,l}$ is that of the condensed phase.

Ethanol density (ρ_E) measured by the IR hydrocarbon detector and the gas temperature (T) measured within it are used to calculate the vapor pressure of ethanol, $p_{v,E} = \rho_E \frac{R}{MW_E} T$. From this partial pressure and the measured pressure within the sensor (p_{tot}) the ethanol mole fraction $x_E = \frac{p_{v,E}}{p_{tot}}$ is determined and converted to mass fraction ($w_{E,v}$), which is then

used to calculate ethanol mass flow rate,

$$\dot{m}_{E,v} = w_{E,v}\dot{m}_{eff} \tag{2.2}$$

Reducing $\dot{m}_{eff}$ by $\dot{m}_{E,l}$ to account for condensation had a negligible effect (¡0.5 % of total mass balance.)

The numerical derivative of the scale reading (i.e., total amount collected) is taken using a first order finite-difference method. The resultant mass flow rate ($\dot{m}_{E,l}$) is then smoothed using a 10 s moving average filter, and the added to the mass flow rate measured in the vapor phase, as per Eq. 2.1.

The second method of extraction rate measurement is to compare the instantaneous flow rate into and out of the extraction vessel using the two Coriolis flow meters. The difference between these two readings is the the extraction rate,

$$\dot{m}_E = \dot{m}_{eff} - \dot{m}_C. \tag{2.3}$$

Though the Coriolis flow meters are more accurate and their uncertainty is small compared to $\dot{m}_E$, they cannot be reliably used to measure the transient extraction rate at this time. The relatively large volume of compressible fluid between the two flow meters acts as a damper, and because the meters are so sensitive, small changes in flow rate measured at one meter (due to valve adjustment, temperature, or pressure changes) not seen at the other meter are erroneously registered as changes in instantaneous ethanol extraction rate. The measured extraction rate according to the Coriolis flow meters is compared to the same measurement according to the IR and scale data in Figure **??**. Even with 60 second moving-average smoothing function applied, the Coriolis based measurement is too noisy to be reliably used as a transient measurement method.

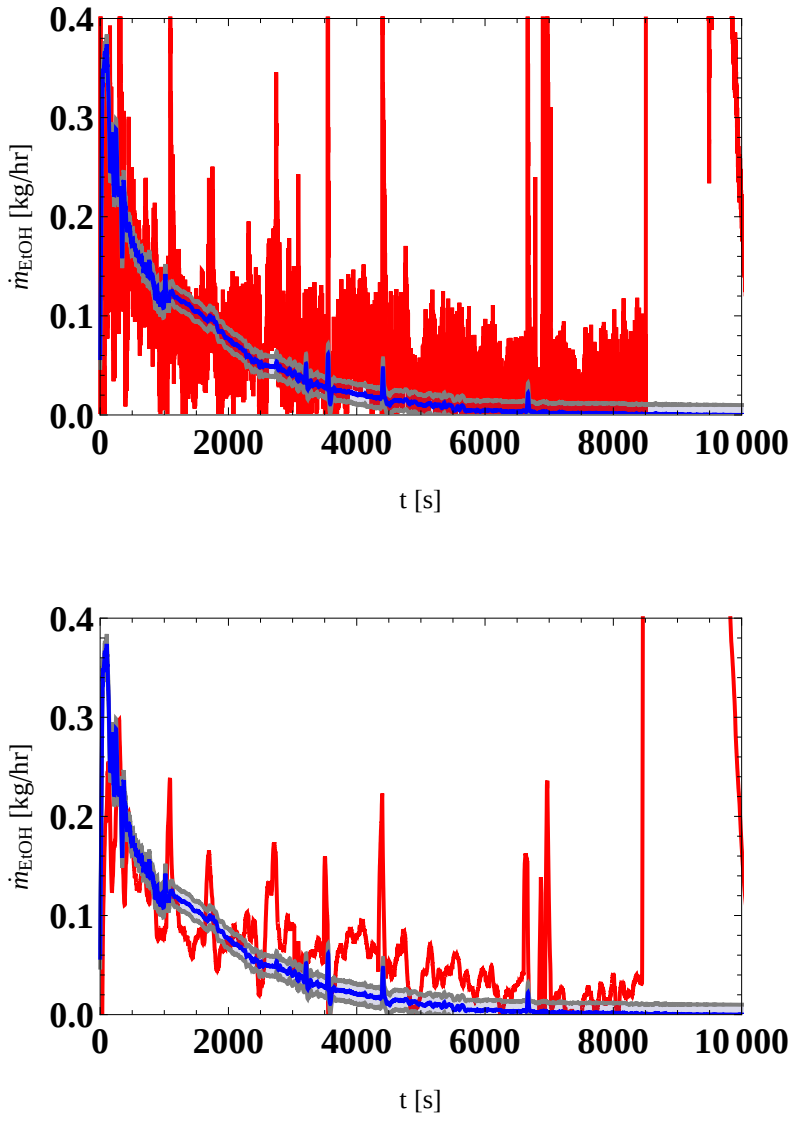

Figure 2.3: Ethanol extraction rate as measured by Coriolis flow meters (red) and effluent sensors (blue). In the bottom figure the Coriolis-based flow rate has been smoothed using a 60 second filter, while the top figure shows the raw measurement.

2.5.2 Drying Time

Required drying time is defined as $t_r = t_f - t_i$. The start time, t_i , is the time at which the decompression valves were first opened. The end of the extraction process (t_f) is determined by taking a running 60-second average of the ethanol mass fraction in the effluent. When this value first drops below 0.0005, the drying process is considered complete.

2.5.3 Total mass extracted

Total mass of ethanol extracted is also calculated using both measurement techniques, and compared to the overall change in mass of the gel and attached mandrel, which is weighed before and after the drying process using an Ohaus Scout Pro digital scale (accurate to ± 0.5 g) as a means of verifying the the overall accurcy of the sensors. Integrating Eq. 2.1, M_E is calculated

$$M_{E,IR} = \sum_{t=t_i}^{t_f} \dot{m}_E \Delta t \tag{2.4}$$

where Δt is the time between measurements (0.2 s at 5 Hz).

The Coriolis flow meter based calculation of total mass extracted is similar, however the limits of summation are different. Fluctuations in flow rate at either flow meter can imply a false value of ethanol extraction rate on short time scales. However, over the course of the entire experiment, from the beginning of pressurization to the end of depressurization, these errors should sum to zero. Therefore the total mass is calculated using the following equation:

$$M_{E,cor} = \sum_{t=t_p}^{t_d} (\dot{m}_{eff} - \dot{m}_C) \Delta t \tag{2.5}$$

where t_p is the start of the pressurization phase and t_d is the end of the depressurization phase.

2.6 Uncertainty Analysis

The uncertainty associated with each primary measurement variable is presented in Table 2.1.

Table 2.1: Measurement uncertainty of primary variables

Variable	**Range**	**Meter**	**Uncertainty**
T	-50 °C to 200°C	T-Type Thermocouple	± 1.0 °C or 1.5%
p	0 MPa to 20.6 MPa (gauge)	Omega PX-309	± 0.25 % of FS
$p_{T,IR}$	0 MPa to 0.206 MPa (gauge)	Omega PX-209	± 0.25 % of FS
$\dot{m}$	0 kg/hr to 15 kg/hr	Siemens Coriolis flow meter	± 1% of reading
ρ	0 kg/m^3 to 2900 kg/m^3	Siemens Coriolis flow meter	± 1 kg/m^3
ρ_E	0 kg/m^3 to 0.090 kg/m^3	SEC Millenium	± 4.5 mg/L
m	0 g to 2000 g	Ohaus Digital Scale	± 0.05 g

In order to determine the experimental uncertainty of derived variables the Kline-McKlintock [**?**] method was applied. The resulting combined errors are presented in Table 2.2

Table 2.2: Measurement uncertainty of derived variables

Variable	**Meaning**	**Maximum Uncertainty**
$w_{E,v}$	EtOH mass fraction (IR meter)	± 0.0025
$w_{E,c}$	ETOH mass fraction (Coriolis)	± 0.0014
$\dot{m}_{E,v}$	EtOH Extraction Rate (IR meter)	± 0.0025$\dot{m}_{eff}$
$\dot{m}_{E,v}$	EtOH Extraction Rate (Scale)	± 25 g/hr
$\dot{m}_{E,C}$	EtOH Extraction Rate (Coriolis)	± 0.0014 $\dot{m}_{CO_2}$

CHAPTER III

Mathematical Modeling

When modeling alcogel drying it is commonly assumed that mass transport within the gel is purely diffusive, that the diffusion coefficient is constant, and that alcohol concentration at the surface of the gel is zero. A notable exception to this is the model by Mukhopadyay and Rao [**?**] who proposed that swelling of the pore liquid results in expulsion of alcohol from the gel and accounted for composition-dependent diffusivity. To investigate these assumptions two models derived from first principles are presented herein. The first is a one-dimensional model representative of a single pore, in which mixture density and diffusivity are composition dependent. The second model is a two-dimensionsional axisymmetric conjugate mass transfer model representing an annular sheet of alcogel with ethanol-absorbing $SCCO_2$ flowing over the outer face of it in which the diffusion coefficient is composition dependent.

3.1 Constitutive Equations for Fluid Properties

The equation for mixture density as a function of composition was developed based on high-pressure density data published by Pohler and Kiran [**?**], and Zúñiga-Moreno and Galica-Luna [**?**]. Density at relevant conditions was interpolated over a range of compositions and a second-order polynomial was fit to these data.

At the pressure and temperature investigated, experimental values for the diffusion co-

efficient are not available, so a constitutive equation was generated from semi-empirical correlations. Strictly speaking, a diffusion coefficient is valid for a negligible amount of solvent diffusion into an essentially infinite solvent. In most engineering applications, this assumption can be relaxed up to a maximum of 5 % to 10 % solute mole percent. To estimate the diffusion coefficient of a binary system across the entire composition range, one must first determine the infinite-dilution diffusion coefficients, i.e. those for a negligible amount of each species into an infinite amount of the other. A function is then applied to connect these two terminal values

Liquid diffusion theory is generally based on the Stokes-Einstein model, essentially a hydrodynamic argument, in which one considers a large solute molecule diffusing through a sea of much smaller solvent molecules. Various semi-empirical correlations have been developed based on this theory, with correction factors to account for the case when the solute and solvent molecules are similar in size. Of these correlations, Reid *et al.* [**?**] found the Tyn-Calus method (Eq. 3.1) [**?**] to have the lowest average error and recommend it's use in most cases,

$$D^o_{CE} = 8.93 \times 10^{-8} \left(\frac{V_C}{V_E^2}\right)^{1/6} \left(\frac{P_E}{P_C}\right)^{0.6} \frac{T}{\mu_E}. \tag{3.1}$$

To account for intermolecular forces, the ratios of molecular volumes (V) *at the normal boiling point* and of parachors (P) are included. The parachor, a derived quantity related to surface tension, density, and molecular weight was estimated using structural contributions as tabulated by Quayle [**?**], and ethanol viscosity, μ_E was interpolated from experimental data by Tanaka *et al.* [**?**] Using this method a diffusion coefficient of $D^o_{CE} = 3.3 \times 10^{-9}$ m^2/s was obtained for the case of infinitely dilute $SCCO_2$.

Diffusion in supercritical fluids is subject to special consideration, since its behavior is characteristic of neither a gas nor a liquid. Methods exist to calculate diffusion in supercritical fluids by either applying a pressure correction to a low-pressure diffusivity (based on gas-diffusion theory) or by using liquid diffusion theory, though the error in these methods

is often quite high [**?**]. A simple and accurate correlation was developed specifically for supercritical fluids by He and Yu [**?**], based on the idea presented by Cohen and Turnbull [**?**] that diffusion in dense fluids occurs by movement of solute molecules into sufficiently large voids between solvent molecules. The correlation was tested against 1303 experimental data points for 113 binary systems (including organic liquids in $SCCO_2$), and the average deviation was 8.2 %.

$$D^o_{EC} = \alpha \times 10^{-5} \left(\frac{T}{M_E} e^{\frac{-0.3887}{V_{rC} - .023}} \right) \tag{3.2}$$

$$\alpha = 14.882 + .005908 \frac{T_{cC} V_{cC}}{M_C} + 2.0821 \times 10^{-6} \left(\frac{T_{cC} V_{cC}}{M_C} \right)^2$$

The critical temperature and molar volume of CO_2 are T_{cC} and V_{cC}, respectively. MW_C is the molecular weight of CO_2, and V_{rC} is the reduced molar volume. An infinite dilution diffusivity of $D^o_{EC} = 2.646 \times 10^{-8}$ m^2/s was calculated using this correlation.

Since the infinite-dilution values for diffusivity change by approximately one order of magnitude depending on which species is the solute and which is the solvent, some care must be exercised in choosing a function to fill in the intermediate concentration range. Though in some ideal mixtures the diffusion coefficient may change linearly with composition, this is not always the case. One method which is often recommended is the Vignes relation:

$$D_F = \left(D^o_{EC}\right)^{1-x_E} \left(D^o_{CE}\right)^{x_E} \alpha. \tag{3.3}$$

This method was also used by Mukhopadyay and Rao [**?**], who assumed the thermodynamic activity factor, α to be unity. In the absence of a value for this activity factor, this assumption was also made in the present study. This omission will, if anything, underestimate the non-ideal behavior of the mixture.

3.1.1 Single Pore Compressible Model

Ethanol transport in the case of composition dependent density and diffusivity was investigated in a single pore model. The pore is considered as a straight walled cylinder with one closed end and one open end. Assuming a slip boundary condition along the pore wall, the problem is reduced to one dimension, the axial direction. Equations for conservation of species, mass, and momentum are solved simultaneously for species, velocity, and pressure. Boundary conditions at the closed end prescribe velocity and species flux equal to zero. At the open end ethanol concentration is set to zero, and pressure to the extraction pressure. Initially, the pore is assumed to be filled with ethanol at rest.

Transient simulations were compared to an incompressible (diffusion only) model and a constant-diffusivity model. Comparison of the composition profile along the pore indicated that in the first 60 s advective transport rates were greater than or equal to diffusive transport rates (i.e. the Peclet number was greater than 1). However this advective period was brief with respect to the total time required for complete drying and had a negligible effect on the overall drying profile. The influence of the changing diffusion coefficient was much more substantial and is therefore considered in the 2-D model.

3.1.2 Annular Sheet Incompressible Model

The concentric annular alcogel and flow gap are modeled in a 2-D axisymmetric COMSOL model (shown in Figure 3.1) considering conjugate mass transfer by diffusion within the gel and combined diffusion and advection in the gap. Throughout the entire domain ethanol transport is governed by the equation for conservation of species,

$$\frac{\partial w_E}{\partial t} + u\nabla w_E = \nabla[D_F \nabla w_E]. \tag{3.4}$$

The entire system is assumed to be isothermal, isobaric, and constant density. In the gel subdomain (L = 220 mm, r_1 = 23 mm to r_2 = 28 mm) the bulk velocity, u, is set

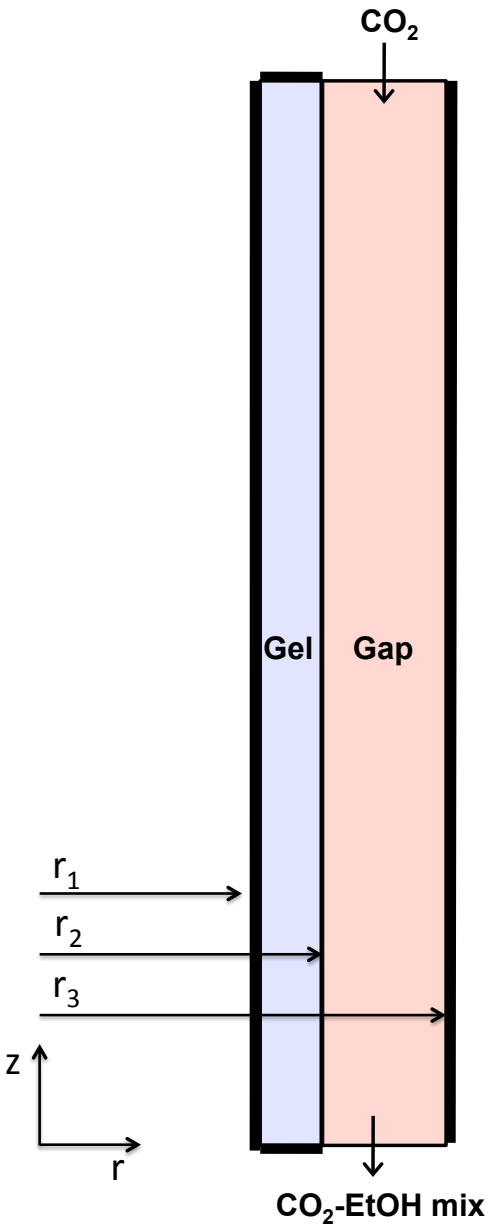

Figure 3.1: Schematic of 2-D axisymmetric model.

equal to zero. In the gap (L = 220 mm, r_2 = 28 mm to r_3 = 38 mm), the Reynolds number ($Re_{Dh} = uD_h\rho/\mu$) is 315 and the hydrodynamic entry length ($x_e = 0.06D_hRe$) is 370 mm (at the maximum experimental flow rate of 5 kg/hr), so flow is laminar and hydrodynamically developing, the velocity field is solved for numerically (assuming a constant inlet velocity and density) before solving the transient species transport problem. Initially, the gel is assumed to be completely ethanol-filled (i.e., w_e=1) with pure CO_2 in the gap. The diffusion coefficient D_F in both subdomains is defined in Equation 3.3. Diffusive transport is assumed to occur through normal molecular diffusion only, i.e., surface diffusion and Knudsen diffusion terms are not considered. Furthermore, diffusion is assumed to be unaffected by the gel structure, and no correction is made for tortuosity or porosity.

Impermeable wall boundary conditions are applied at the three sides on the gel subdomain not in contact with the flow gap ($z = 0$, $z = L$, $r = r_1$), as well as the side of the gap subdomain opposite the alcogel ($r = r_3$). At the flow inlet ($z = L$) the fluid is assumed to be pure CO_2 (i.e. $w_E = 0$), and at the outlet ($z = 0$) the species gradient is assumed to be zero. Finally, at the internal boundary between the alcogel and flow gap subdomains, continuity is applied (i.e. species and species gradient are set equal). Initially the the alcogel is assumed to be completely ethanol-filled ($w_E = 1$), and the flow pure CO_2.

Mass flow rate of ethanol from the outlet is defined by

$$\dot{m}_E = \int_{r_2}^{r_3} w_e \rho u 2\pi r dr$$

A scaling factor (W) is used to adjust the model to each particular experiment, where W is the ratio of the measure change in mass to the predicted amount extracted based on the model:

$$W = \frac{M_{E,TOT}}{\int_0^\infty \dot{m}_E dt}. \tag{3.5}$$

The corrected flow ethanol extraction rate is then defined as:

$$\dot{m}_{E,scaled} = W\dot{m}_E \tag{3.6}$$

This scaling factor allows the model to accommodate variation in the total mass extracted as a result of damage to the gel during casting, providing the characteristic dimensions of the system are not changed.

CHAPTER IV

Results and Discussion

A series of alcogels drying experiments were performed by varying CO_2 mass flow rate from 1 kg/hr to 5 kg/hr in 1 kg/hr intervals while maintaining pressure and temperature at 12.7 MPa and 50 °C respectively. Each experiment was performed in duplicate. Total mass balance results are presented in Table 4.1. The representative CO_2 mass flow rate for each experiment is the time average of CO_2 mass flow rate over the "stable" portion of the run (from the time that target flow rate is reached until decompression begins). Effluent vapor and effluent condensed are the amount of mass measured by the IR sensor effluent scale, respectively, and effluent total is the sum of these. (The is also shown graphically in Figure 4.1.) The error bounds on this measurement correspond to the error of the IR sensor -based measurement, integrated over the course of the run. This compared to the total mass extracted according the the Coriolis flow meters, and difference in mass of the gel + mandrel assembly before and after drying.

4.1 Effect of CO_2 Flow Rate

Typical ethanol extraction rate curves at each flow rate are shown Figure 4.1. Generally, in the first phase of the drying process, approximately the first 20 minutes, the ethanol extraction rate is relatively high, nearly 10 % of the total effluent flow rate. After this initial surge, the extraction rate drops substantially and continues to decrease slowly and at

Table 4.1: Total mass of ethanol extracted as measured by each technique at a range of CO_2 flow rates

CO_2 Flow Rate [kg/hr]	**Effluent Vapor** [g]	**Effluent Condensed** [g]	**Effluent Total** [g]	**Coriolis** [g]	**Expected** [g]
0.99 ± 0.14	76.1± 10	32.4	108.5± 10	149.5 ± 11.5	119.7
1.00 ± 0.04	72.1± 9.1	27.5	99.6± 9.1	107.5± 11.3	112.7
1.90 ± 0.08	77± 11	25.7	102.7± 11	117.6 ± 13.2	111.5
1.87 ± 0.23	93.4 ± 12.1	17.3	110.7± 12.1	112.9± 14.1	122.6
2.87 ± 0.21	104 ± 18	22.2	126.2± 18	128.2± 16.2	124.9
2.87 ± 0.17	102.7 ± 22.7	22.2	124.9± 22.7	147.4 ± 19	124.2
3.78 ± 0.24	85.5± 16.5	20.3	105.8± 16.5	120.7 ± 16.4	106.1
3.90 ± 0.12	88.6± 17.6	27.3	115.9± 17.6	144.1 ± 21	122.8
4.75 ± 0.55	79.2 ± 20	33.2	112.4± 20	135.6 ± 22.8	121.0
4.76 ± 0.30	79.2 ± 22.5	33.7	112.9 ± 22.5	135 ± 22.8	120.9

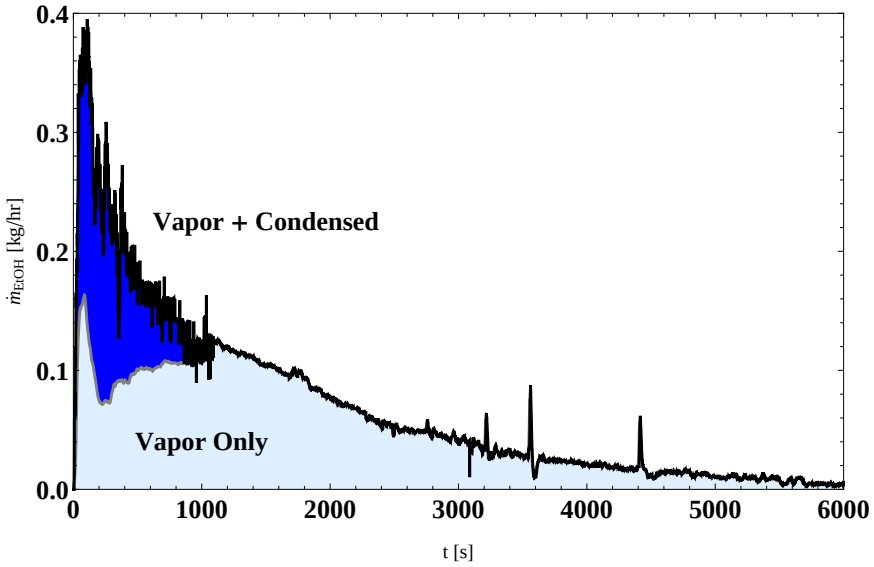

Figure 4.1: Typical mass flow rate of ethanol measured in the effluent at 3.90 kg/hr CO_2 flow rate

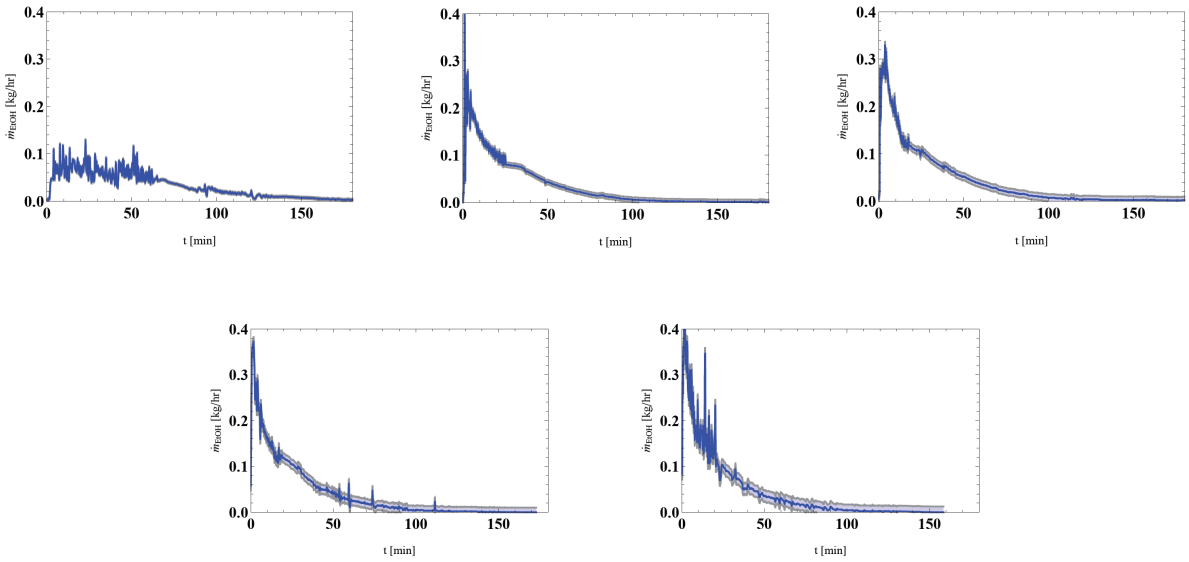

Figure 4.2: Representative ethanol extraction rates at each CO_2 flow rate. First row: 1.0 kg/hr, 1.9 kg/hr, and 2.9 kg/hr. Second row: 3.9 kg/hr, and 4.75 kg/hr

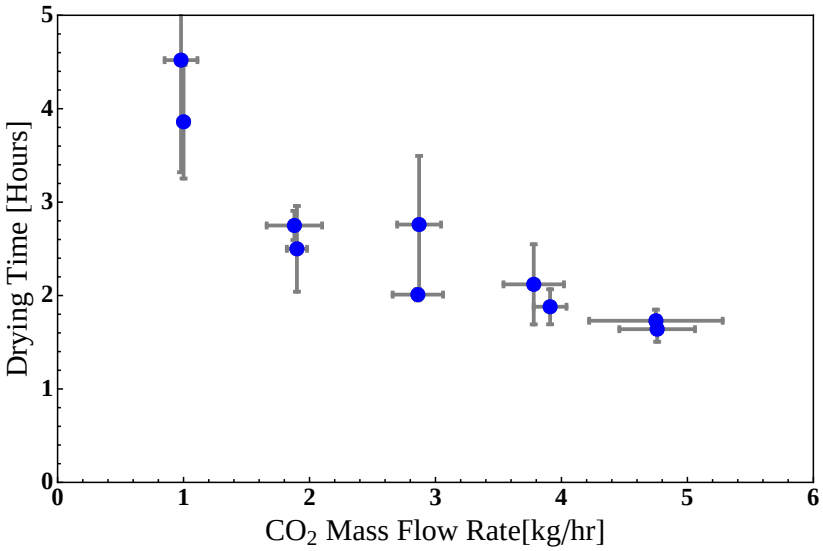

Figure 4.3: Drying time based on when w_E in the effluent first reaches zero for a range of CO_2 mass flow rates (representative flow rate is the average flow rate over the course of the experiment). Error bars corresponding to flow rate indicate one standard deviation. Error bars in time indicate the error as measured by the the effluent IR sensor.

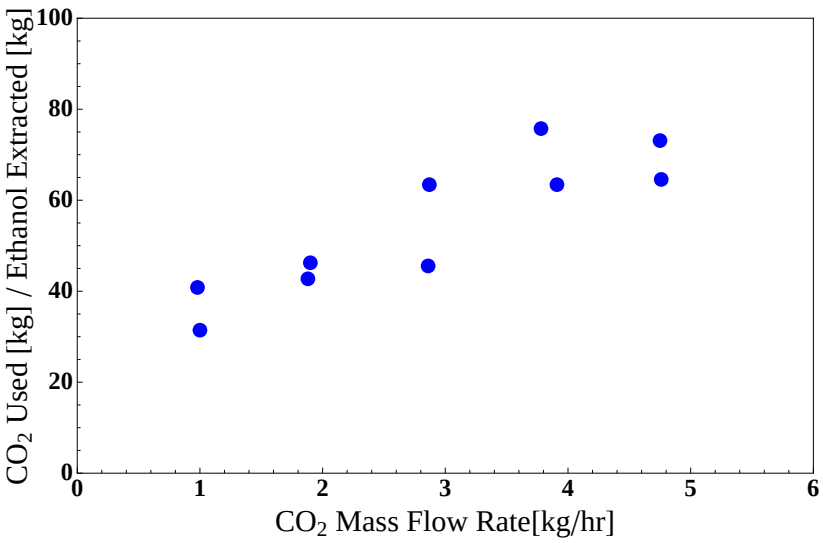

Figure 4.4: CO2 used per kg ethanol extracted

a near-constant rate for the duration of the run. As CO_2 flow is increased, the magnitude of this initial surge increases, however, after the initial surge the subsequent rate of decrease is relatively independent of CO_2 flow rate. The exception is the 1 kg/hr case, which has no initial spike, but rather a moderate extraction rate for a much longer time. In the higher flow rate runs that had an initial spike in flow rate this indicates that the majority of the drying process is diffusion limited, i.e., essentially unaffected by flow rate. In the 1 kg/hr case CO_2 flow becomes more ethanol-rich as it passes over the gel, which decreases the driving force for diffusion and thereby the extraction rate.

The time required to completely dry a gel (as defined in Section 2.5) is also influenced by CO_2 mass flow rate. When the CO_2 flow rate is low, it can take significantly longer to remove all the ethanol from the gel. Initially, increasing the flow rate results in a dramatic decrease in required drying time (e.g., 4.2 hours at 1 kg/hr to 2.6 hours at 2 kg/hr). However, the marginal benefit decreases with each increase in flow rate, and indeed it seems that above some limit, increasing flow rate has no noticeable effect. Though increasing CO_2 flow rate can reduce process time, this reduction is insufficent to offset the additional amount of CO_2 used. As shown in Figure 4.4, the mass of CO_2used per mass of ethanol extracted monotonically

increases with flow rate.

The preceding results indicate the drying process could be optimized in terms of minimizing both process time and CO_2 usage by using a varying flow rate. Early in the extraction process, when ethanol extraction rates are quite high, a higher CO_2 flow rate would lead to increased extraction. After this initial period the CO_2 flow rate could presumably be reduced without substantially decreasing the extraction rate, thus conserving CO_2.

4.2 Comparison to Conjugate Mass Transfer Model

Experimental extraction rate results are compared predictions of the model described previously, as shown in Figure 4.5. The model captures the general behavior of the drying process in terms of overall magnitude and trend, if not the specific extraction rates. Specifically, initial extraction rates (say, the first few minutes of the process) are underestimated, leading to a subsequent overestimation of the extraction rate, followed by a period of relative agreement. This could be attributed in large part to the difference in initial conditions between the model and experiments. At $t = 0$, the model consists of two separate regions, one purely ethanol and the other purely CO_2. In reality, the system is unable to sustain this species discontinuity preceding the technical start of the extraction phase. During pressurization, some amount of ethanol mixes with the surrounding CO_2, and when the outlet is opened, this ethanol-rich mixture leaves the vessel. After the initial spike there is consequently slightly less ethanol in the gel, and the concentration gradient is decreased, so the diffusive extraction rate is decreased.

Figure 4.6 compares the estimated amount of ethanol extracted vs. the amount measured in the effluent. As observed in the extraction rate comparison, the model under-predicts extraction early in the drying stage, then over-predicts it later to compensate. However, the effect of this omission is relatively minor in terms of the total mass that has been extracted at any given time, as the simulation and experimental measurement agree to within 10 % over the entire course of the drying process.

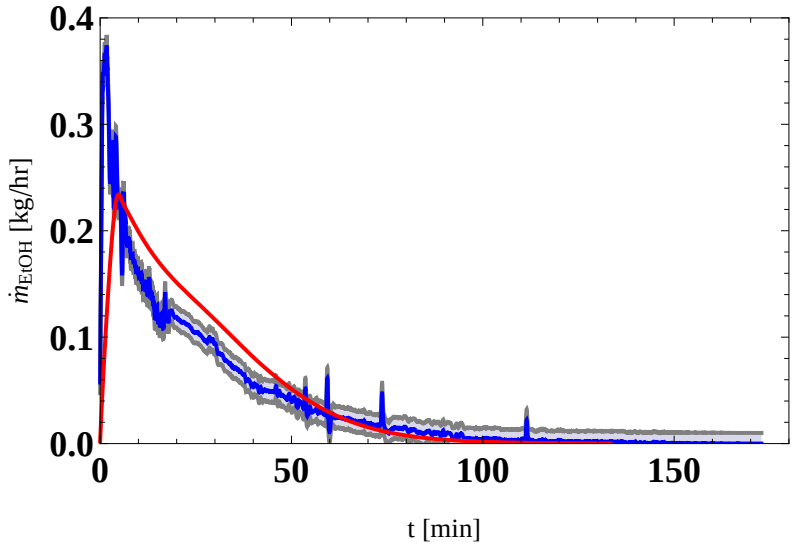

Figure 4.5: Ethanol mass extraction rate as measured by combined vapor and liquid effluent sensors (blue line, with error in gray) during a 3.90 kg/hr run, and as predicted by the corresponding parallel plate conjugate mass transfer model (red line).

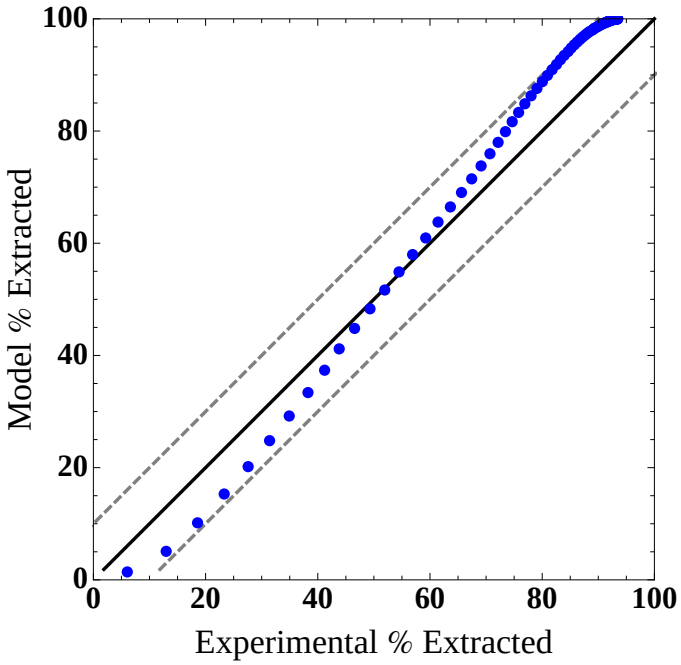

Figure 4.6: Predicted percent ethanol extracted vs. actual percent extracted (at $\dot{m}_C = 3.90$ kg/hr), normalized to the expected total. Dashed lines indicate ± 10%

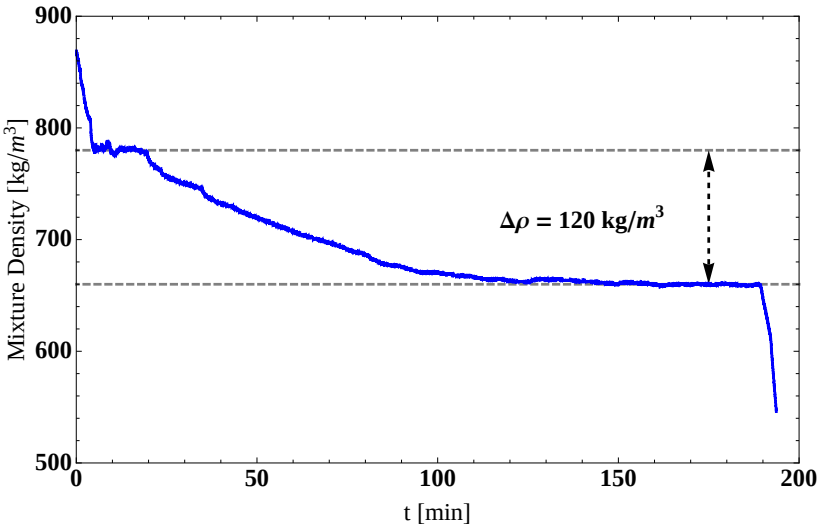

Figure 4.7: Effluent mixture density over the course of a drying run at 2 kg/hr.

4.3 High-Pressure Density Measurement

Mixture density in the supercritical phase, though not presently used as a metric, may be the most accurate method by which to measure extraction rate. The Coriolis flow meter downstream from the pressure vessel continuously measures density to within $\pm$ 1 kg/m^3. Over the course of typical experiment the density change is two orders of magnitude greater than is this (as shown in Figure 4.7), a change predominantly attributed to change in mixture composition, as temperature and pressure fluctuations are minor. However, in order to accurately determine ethanol content and extraction rate the dependence of mixture density on pressure, temperature, and composition must be known, and in this respect experimental data and predictive equations of state are still lacking. A detailed study of the density's dependence on these variables over the relevant composition range would facilitate the verification and implementation of this technique.

CHAPTER V

Conclusions and Future Work

An apparatus and method to continuously measure the ethanol extraction rate during supercritical CO_2-based drying of silica alcogels as a function of various drying parameters has been presented. The extraction process was shown to be largely diffusion limited, except at low flow rates when the mass transfer driving force is decreased by excessive ethanol buildup in the CO_2 flow. Beyond the range where this buildup effect is significant, the process is relatively insensitive to flow rate, except in the beginning of the drying process, where extraction rate can be increased by increasing flow rate.

A parallel plate model of the annular experimental drying setup was developed assuming a composition-dependent diffusion coefficient within the gel with laminar developing CO_2 flow over it. Advective transport within the gel, i.e., "spillage" was not considered. The transient extraction rate predicted by this was in good agreement with experimental data for the majority of the run, and the predicted amount extracted at any given time was typically within 10 % of the measured amount. Disagreement between the predicted and measured ethanol extraction rate at the beginning of the process is attributed to the initial condition of the model, in which the gel subdomain is purely ethanol, and the surrounding fluid is pure $SCCO_2$, with a step discontinuity at the interface. In the real system some of the ethanol diffuses into the surrounding fluid during pressurization, changing the composition of the effluent at first.

The results presented herein provide the foundation for future experimental and modeling work. The most immediately feasible is to continue using the experimental rig to investigate the effect of other drying parameters on extraction time. Temperature, pressure, gel thickness and gap spacing can be investigated without requiring any modification to the system. Extraction rate from alcogels initially filled with a different solvent (e.g. methanol) could be measured by simply replacing the IR sensor with a model specific to that solvent. Moving forward, efforts should be made to develop the use of mixture density as a metric by which to measure extraction rate. One critical development which would facilitate this is the precise measurement of density as a function of composition at specific pressure and temperatures. Alternatively, an equation of state which is highly accurate over the relevant range would suffice. Another important improvement which could be made to the experimental apparatus is a means by which to reduce fluctuation in flow rate upstream from the extraction vessel. This would allow the Coriolis flow meter measurements to be used to measure instantaneous ethanol extraction rate. A number of improvements can be made to the numerical model as well. Modification to account for the pressurization stage (and therefore better approximate the initial condition of the experiment) should be made. Complexity can also be added to account for the effect of the silica structure and chemical activity coefficient on the diffusion coefficient.

BIBLIOGRAPHY